Elevation dependence of cosmogenic ^{36}Cl production in Hawaiian lava flows

Darin Desilets [*], Marek Zreda [1]

Department of Hydrology and Water Resources, University of Arizona, Tucson, AZ, 85721, USA

Abstract

We measured an elevation profile of cosmogenic ^{36}Cl in two well-preserved lava flows on Mauna Kea, Hawaii (19.8° N, 155.5° W) in order to directly constrain the elevation dependence of cosmogenic nuclide production rates. The flows are vertically-extensive hawaiites erupted at 40.1 ± 0.6 and 62.2 ± 1.0 ka from point-vents on the upper flanks of Mauna Kea. The average paleo cutoff rigidity (a measure of geomagnetic shielding of cosmic rays) for these flows is 11 GV and their paleo-elevation range is 2100–3700 m. Production of ^{36}Cl is dominated by neutron reactions, with the high-energy ^{39}K(n,x) and ^{40}Ca(n,x) mechanisms accounting for nearly half of the ^{36}Cl production and the low-energy reaction ^{35}Cl(n,γ) responsible for the remaining half. Production by negative muons is small at the elevations of our samples, accounting for less than 2% of the total production in the lowest elevation samples. The elevation dependence of ^{36}Cl production measured in these lava flows is described by an effective attenuation length of 138 ± 5 g cm^{-2}. This result is close to the value of 140 g cm^{-2} determined from neutron monitor surveys of high-energy nucleon fluxes, but significantly below the value of 149 g cm^{-2} determined from measurements of low-energy neutrons. The predicted atmospheric attenuation length for these lava flows, incorporating both high- and low-energy mechanisms, is 144 g cm^{-2}. The good agreement between the ^{36}Cl elevation profile and cosmic-ray surveys validates the use of neutron flux measurements to scale ^{36}Cl production rates when production by muons is negligible.
© 2006 Elsevier B.V. All rights reserved.

Keywords: attenuation length; cosmogenic nuclides; scaling factors; Mauna Kea; cosmic rays

1. Introduction

The buildup of cosmogenic nuclides in surface materials can provide quantitative information on the surface exposure history of a wide variety of features including neotectonic, erosional, glacial and depositional landforms [1]. Successful application of cosmogenic nuclides requires knowledge of local production rates, which at the land surface are controlled by the local secondary cosmic-ray nucleon intensity and to a lesser extent by muon intensity [2]. Because nucleon fluxes attenuate rapidly in the atmosphere, production rates are very sensitive to elevation.

The application of calibrated production rates to other sites requires knowledge of the elevation dependence of production rates. Because copious and precise data from neutron monitors and other instruments have long been available [3], data from cosmic-ray surveys have most often been used to infer that dependence [2,4–6]. However, the scaling models derived by

* Corresponding author. Tel.: +1 520 621 4072.
  E-mail address: ddesilet@hwr.arizona.edu (D. Desilets).
[1] Tel.: +1 520 621 4072.

various authors have not been entirely consistent [6], indicating that the use of cosmic-ray measurements can be problematic. One problem is that the spatial distribution of neutron fluxes seems to be energy dependent [6,7], and that instruments such as neutron monitors have an energy sensitivity that is different from the excitation functions for production of most cosmogenic nuclides. Another problem is that ^{36}Cl production rates from slow negative muon capture by potassium and fast muon initiated photodisintegrations in calcium and potassium are not well known, but if significant they would give scaling factors that are less sensitive to elevation than scaling factors based on neutrons alone.

One way of determining the elevation dependence of production rates that avoids the problem of instrumental biases is the direct measurement of nuclide production in artificial targets [8–10]. Most recently, that approach was successfully applied to measure ^{10}Be, ^{3}He and ^{3}H production in water targets [10] over an elevation profile spanning 4100 m. A drawback to using artificial targets is that an exposure time on the order of years is required. But for many of the commonly applied nuclides even several years of exposure is insufficient for the accumulation of measurable inventories. New procedures and/or analytical methods must be devised to overcome this problem.

An alternative to conducting neutron flux surveys and exposing artificial targets is the direct measurement of cosmogenic nuclide buildup in natural materials irradiated over a geologic time scale and spanning a significant elevation range. There have been several analogous investigations aimed at directly measuring the depth-dependence of production rates in rock (e.g. [11,12]), but there has been only one study where an atmospheric profile was obtained from surface samples [13], and those results are uncertain due to poor constraints on independent ages. The goal of this work is to provide more accurate and precise data than have been previously available.

Few natural landforms are suitable for measuring cosmogenic nuclide production along an elevation profile. The ideal landform for this type of work would: (1) be of uniform age; (2) cover a substantial elevation range with little change in latitude (cutoff rigidity); (3) contain an abundance of requisite minerals for production and retention of the nuclide of interest; (4) have a long exposure time (sufficient cosmogenic nuclide buildup); and (5) have a simple exposure history (negligible burial or erosion) if long-lived nuclides are to be applied. The well-preserved, vertically extensive lava flows of the Haleakala, Hualalai and Mauna Kea volcanoes make Hawaii one of few locations with landforms that meet all five of these conditions.

Extensive measurements of neutron intensity performed there by us [14] and others [15,16] also make Hawaii an ideal benchmark location for comparing neutron measurements with cosmogenic nuclide production. In this paper we report an altitude profile of ^{36}Cl production in lava flow surfaces on Mauna Kea, Hawaii and we compare those results to the altitude profile predicted from neutron flux surveys.

2. Site description and methods

2.1. Surficial lavas of Mauna Kea, Hawaii

The surficial lavas of Mauna Kea were extruded in two compositionally distinct episodes of post-shield volcanism known as the Hamakua and Laupahoehoe substages [17]. The Hamakua Volcanics are characterized by alkali and transitional basalts erupted between 230 and 65 ka. These flows typically contain less than 10% of olivine, augite and plagioclase phenocrysts. Eruptions of Hamakua basalts were followed by the typically aphanitic hawaiite, mugearite and benmoreite lavas of the Laupahoehoe Volcanics substage, extruded between 65 and 4 ka. Laupahoehoe lavas erupted from vents scattered along the upper slopes of Mauna Kea, mostly covering the Hamakua Volcanics above 1500 m. These eruptions are characterized by aa flows issuing from vents surrounded by 30–100 m high cinder cones. Air-fall deposits (lapilli and ash) are commonly associated with Laupahoehoe eruptions, locally blanketing flow surfaces and forming sheets and dunes of reworked ash [17].

2.2. Climate of the Island of Hawaii

Steep climate gradients on Hawaii mean that the preservation of primary flow features varies drastically across the island. A major factor controlling rates of surface weathering and erosion is precipitation, which is a function of the intensity and direction of the prevailing northeast trade winds. A temperature inversion caps the trade winds at ∼ 1800 m and generally keeps moisture-laden air from reaching the upper slopes of Mauna Kea [18]. Strong local thermal convection over the mountains frequently disrupts the inversion, drawing moisture farther up slope, but rarely results in significant rainfall. Precipitation generally increases with elevation to the height of the inversion, and then decreases [18]. Precipitation rates are highly variable across the island, ranging from 600 cm yr^{-1} on the windward eastern slopes of Mauna Kea to <50 cm yr^{-1} on the leeward slopes. Old lava flow surfaces are best preserved at elevations above 1800 m and on southwest facing slopes.

2.3. Sample collection

We collected samples from Laupahoehoe stage hawaiites erupted on the dry southwestern flank of Mauna Kea above the Humuula Saddle (Fig. 1). We selected two adjacent flows mapped by [19] (referred to in this work as flows L1 and L2), that extend from cinder cones at 3567 and 3206 m to the Humuula Saddle at 1900 m. These flows were selected because of their large elevation range, good to excellent preservation of primary flow features, and estimated age (>16 ka based on surface weathering) which ensures easily measurable ^{36}Cl/Cl. Primary flow features (ropes, tumuli, pressure ridges, channels with levees) are present intermittently over the entire lengths of both flows, although surfaces are less vegetated and better preserved at higher elevations.

Lava flows of the Laupahoehoe substage are nearly identical in appearance and composition, making the distinction of separate flows difficult either in the field or laboratory. Low rates of erosion and of colonization by vegetation further make it difficult to distinguish individual hawaiite flows from separate eruptions, even when ages are different by thousands of years. We observed that because of the elevation/climate gradient, variations in surface preservation are often greater along a flow than they are between flows of different age.

The majority of our samples were collected from levees bordering lava flow channels (Fig. 2). An advantage of sampling levees is that these features tend to be topographically prominent, making prolonged burial by ash unlikely. We sampled only from levees and other features that had ropes or rough popcorn-like texture as evidence of a primary flow surface. Preservation of this intricate flow surface texture suggests that the depth of erosion at these places is less than 2 cm.
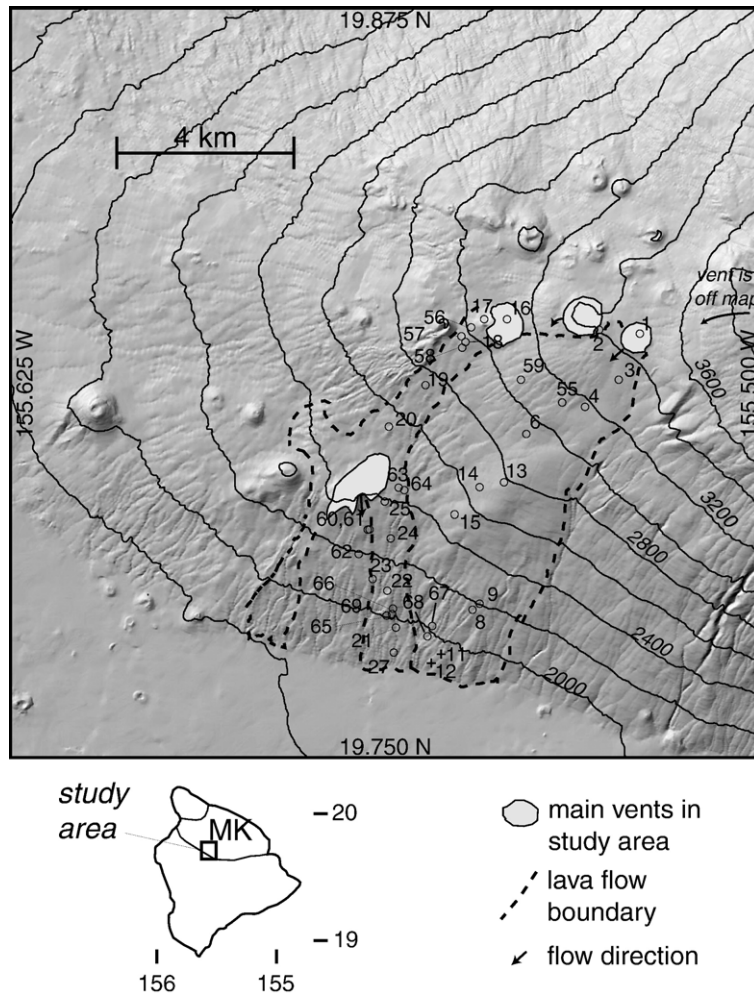

Fig. 1. Study area and sample locations on Mauna Kea (MK).

Fig. 2. Typical lava flow levee on upper slopes of Mauna Kea (sample HAW03-17).

2.4. Laboratory procedures

Whole rock samples were crushed and sieved to the 0.25–1.0 mm size fraction and then leached for 24 h in 5% HNO_3 to remove meteoric Cl. Samples labeled HAW00-L1 were spiked with ^{35}Cl enriched carrier and digested in a high-pressure acid digestion vessel according to the procedure in [20]. Samples labeled HAW00-L2 and HAW03-L1 were digested without carrier in open containers according to [20]. Splits of seven of the HAW00-L1 samples were also digested without carrier in open vessels [20]. Three of the seven splits returned Cl concentrations or $^{36}Cl/Cl$ values that were inconsistent and therefore these samples were discarded from the data analysis. Samples were analyzed for $^{36}Cl/Cl$ by accelerator mass spectrometry (AMS) at PRIME Lab, Purdue University. Analytical errors in $^{36}Cl/Cl$ and $^{35}Cl/^{37}Cl$ were propagated to landform age according to [20]. Results from AMS and from chemical analyses of bulk rock samples are given in Supplemental Tables 1 and 2 (in Appendix A).

3. Age calculations

Three types of landform ages are discussed in this paper: uncorrected, corrected (true) and apparent. Uncorrected ^{36}Cl ages are based on geologically calibrated production rates [21] scaled to Hawaii according to [6] using the current geographic latitude of 19.8° N to calculate the effective vertical cutoff rigidity and calculating atmospheric depth from the modern elevation. The corrected age takes into account time-dependent variations in geomagnetic dipole inten-

sity and sea level and is based on calibrated production rates that are corrected for changes in geomagnetic dipole intensity and position. These new production rates are based on [21]'s recalibration and have values of $P_{Ca}=72.7$ atoms g^{-1} yr^{-1}, $P_K=158$ atoms g^{-1} yr^{-1} and $P_f(0)=665$ neutrons g^{-1} yr^{-1}.

Apparent ages are proportional to the local ^{36}Cl production rate, which depends on elevation. They are calculated by assuming that samples have an elevation of 2600 m, which is approximately the mean elevation for all samples, and by neglecting corrections that depend on the true exposure age (corrections for radioactive decay, geomagnetic field strength and sea level) since these will have proportionately the same effect on all samples from the same lava flow surface. Because apparent ages assume a fixed elevation for all samples, high elevation samples will have older apparent ages than low elevation samples. The purpose for calculating apparent ages is to give a measure of ^{36}Cl production rate that is normalized for variations in the relative concentrations of Ca, K and ^{35}Cl targets for ^{36}Cl production.

3.1. Equations and approximations for numerical age calculations

The buildup of inventory, N, of a nuclide with calibrated production rate, P, and decay constant λ, is governed by the equation

$$\frac{dN}{dt} = f(R_C(t))f(x(t))P - \lambda_N \tag{1}$$

where $f(R_C(t))$ and $f(x(t))$ are scaling factors, also known as the latitude and elevation scaling factors. The scaling

factors scale the calibrated production rate from the cutoff rigidity, R_C, and atmospheric depth, x, of the calibration site, or from an arbitrary datum to which the production rate has previously been scaled (usually sea level and high latitude), to the cutoff rigidity and atmospheric depth of the sample site. The scaling factors are given as a function of time in Eq. (1) because cutoff rigidity and atmospheric depth varied in the past.

The dependence of production rates on atmospheric depth at a given point in time can be described by the exponential relation:

$$f(x) = \exp\left(\frac{x_0 - x}{\Lambda}\right) \tag{2}$$

where $f(x)$ scales production rates between sea level (x_0 [g cm^{-2}]) and the atmospheric depth of the sample site (x [g cm^{-2}]), and Λ [g cm^{-2}] is the atmospheric attenuation length. The atmospheric attenuation length is known to be a function of elevation [7], but because Λ does not change much over the elevations considered in this work we will consider it to be constant with elevation. The latitude scaling factor $f(R_C)$ is given in [6].

The solution to Eq. (1) with time-dependent scaling factors is

$$N = P \int_0^{t_{\exp}} f(R_C(t)) f(x(t)) \mathrm{d}t - \lambda \int_0^{t_{\exp}} N \mathrm{d}t \tag{3}$$

which must be evaluated numerically because $R_C(t)$ and $x(t)$ are nonanalytic. In order to make Eq. (1) analytically tractable we made two simplifying assumptions. First, we assumed that the integral of the product of the scaling factors is approximately equal to the product of the average scaling factors:

$$\int_0^{t_{\exp}} f(R_C(t)) f(x(t)) \mathrm{d}t$$
$$\approx \frac{1}{t_{\exp}} \int_0^{t_{\exp}} f(R_C(t)) \mathrm{d}t \cdot \frac{1}{t_{\exp}} \int_0^{t_{\exp}} f(x(t)) \mathrm{d}t \tag{4}$$

This approximation is valid when temporal variations in either $f(R_C(t))$ or $f(x(t))$ are small enough or when changes are periodic and the period is much shorter than the integration time. Second, we assume that the average altitude and latitude scaling factors can be calculated from the average values of R_C and x over the exposure period:

$$\frac{1}{t_{\exp}} \int_0^{t_{\exp}} f(R_C(t)) \mathrm{d}t \approx f\left(\frac{1}{t_{\exp}} \int_0^{t_{\exp}} R_C(t) \mathrm{d}t\right) = f(\overline{R_C}) \tag{5a}$$

$$\frac{1}{t_{\exp}} \int_0^{t_{\exp}} f(x(t)) \mathrm{d}t \approx f\left(\frac{1}{t_{\exp}} \int_0^{t_{\exp}} x(t) \mathrm{d}t\right) = f(\overline{x}) \tag{5b}$$

This approximation is valid if the altitude and latitude scaling factors are linearly related to x and R_C, which is approximately the case when changes in R_C and x are small enough. Eq. (1) can then be written as

$$\frac{\mathrm{d}N}{\mathrm{d}t} = f(\overline{R_C}) f(\overline{x}) P - \lambda N \tag{6}$$

and the solution evaluated over $t_{\exp}$ is

$$t_{\exp} = \frac{-1}{\lambda} \ln\left(1 - \frac{\lambda N}{f(\overline{R_C}) f(\overline{x}) P}\right) \tag{7}$$

where the values of $t_{\exp}$, $f(\overline{R_C})$ and $f(\overline{x})$ are interdependent and therefore must be determined iteratively. Eqs. (6) and (7) apply only for $t \ll 1/\lambda$. For exposure times on the order of $1/\lambda$, the scaling factors must be exponentially weighted so that values from earlier in the exposure period contribute less. Corrected ages in this work were calculated using Eq. (7) since exposure ages are fairly young compared to the half-life for ^{36}Cl. Any systematic errors related to the simplifications in Eq. (7) are probably much smaller than errors associated with reconstructions of past cutoff rigidities and past atmospheric depths at the sample site.

For older landforms it is necessary to account for radioactive decay in calculating the time-integrated scaling factors. This can be accomplished by taking the convolution integral of the decay function and the time-dependent scaling factor:

$$f(\overline{R_C})^* = \frac{1}{t_{\exp}} \int_0^{t_{\exp}} f(R_C(t)) \cdot \exp(-\lambda(t_{\exp} - t)) \mathrm{d}t \tag{8a}$$

$$f(\overline{x})^* = \frac{1}{t_{\exp}} \int_0^{t_{\exp}} f(x(t)) \cdot \exp(-\lambda t(t_{\exp} - t)) \mathrm{d}t \tag{8b}$$

where $f(\overline{R_C})^*$ and $f(\overline{x})^*$ are the decay-corrected scaling factors which replace $f(\overline{R_C})$ and $f(\overline{x})$ in Eq. (7).

Corrected lava flow ages were calculated according to the following steps. First, sample ages were calculated from Eq. (7) and the scaling model in [6,16]. These initial age estimates were plotted as a frequency histogram, which (as discussed in Section 4.1), ultimately served as the basis for distinguishing individual flows. Flow ages were calculated from a weighted average of all of the individual ages within a histogram peak. Sample ages were then iteratively recalculated from the latitude scaling in [6] but using the attenuation length determined from the elevation profile itself (Section 4.2). The final corrected lava flow age

reflects a single paleo R_C and paleo elevation determined from the mean age of the flow.

3.2. Paleo R_C

Cutoff rigidity (R_C) was calculated for each time step using paleomagnetic records to determine paleo-geomagnetic latitude (λ_m) at Mauna Kea and by converting λ_m to R_C according to [6]. We used [22]'s marine record of geomagnetic field intensity for the period 12–800 ka and the more detailed archeomagnetic record [23] for the period 0–12 ka, and we assumed that the geocentric axial dipole hypothesis is valid. Time-averaged R_C values were calculated by numerically integrating R_C over 500 yr intervals from 0–4 ka and over 1000 yr intervals from 4–800 ka. This calculation is iterative because the determination of exposure age requires knowledge of the temporally-averaged R_C and x, which are in turn functions of exposure age.

3.3. Paleo atmospheric pressure

Mauna Kea has been slowly subsiding relative to sea level at a rate of ~2.6 mm year^{-1} [24] from the weight of the Hawaiian volcanoes depressing the oceanic crust. Subsidence of the island means that our sample sites were on average 50–80 m higher over the past 40–65 ka compared to their present elevations, and therefore, the average paleo-atmospheric pressures over Mauna Kea were lower. Production rates were consequently higher in the past, on average by 3–6%.

We used daily radiosonde data from Hilo International Airport over the period 1998–2002 [25] to determine the relation between elevation and air pressure on Mauna Kea (Fig. 3). Although there is evidence for a substantially different past climate in this area (e.g., well-preserved terminal moraines on Mauna Kea), suggesting the possibility of a different paleo-atmospheric pressure structure in this area, the use of modern, local pressure–elevation relationships (e.g., [26]) probably improves the accuracy of scaling factors for locations where more generic relations such as the ICAO International Standard Atmosphere (ISA) [27] are inaccurate. The fact that the sea-level atmospheric pressure (1998–2002) in January is greater on average than the July pressure by only 1.5 g cm^{-2} (~1% difference in production rate) implies that the pressure structure could have been similar even during periods of cooler climate, although this assumption would be difficult to support without precise paleo-barometic data. Using the standard values for sea-level pressure
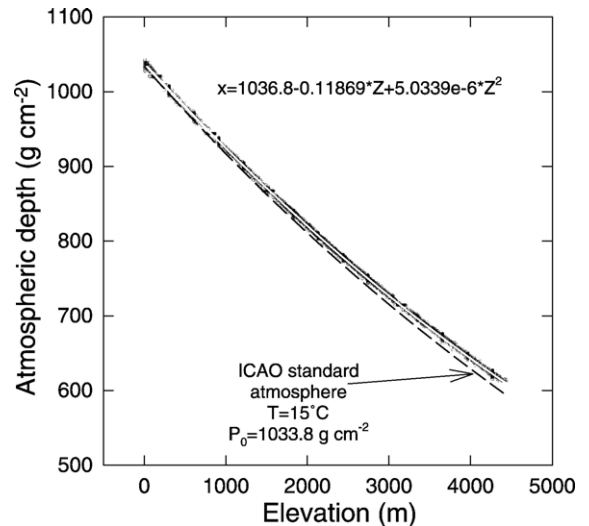

Fig. 3. Best fit (white line) to atmospheric pressure data recorded by daily radio soundings at Hilo, Hawaii, 1998-2002 (circles). ICAO International Standard Atmosphere (black line) shown for comparison.

(1033.8 g cm^{-2}), sea-level temperature (15 °C) and dry adiabatic lapse rate (6.5 °C km^{-1}), the ISA model gives a pressure at 4400 m that is 15 g cm^{-2} lower than the 5-year average pressure recorded by radiosonde at that altitude, which corresponds to a production rate that is higher by 11%. The difference in production rates is reduced to 2% if the current average annual sea-level temperature (23.9 °C) and pressure (1036.8 g cm^{-2}) at Hilo are used instead of the standard values. This demonstrates that the ISA model is a reasonable approximation at Hawaii and possibly other tropical locations, but only if local sea-level temperature and pressure are used instead of the standard values. In this work, we used the regression in Fig. 3 to calculate atmospheric depth from the elevation data after correcting the elevation recorded in the field for subsidence [24].

4. Results and discussion

4.1. Using ^{36}Cl ages to distinguish lava flows

Our results indicate that flow boundaries for L1 and L2 are more complex than is suggested by the most recently published geologic map [19]. A first approximation to the age distribution shows two distinct peaks (Fig. 4), indicating two separate flows. However, the field locations of the samples constituting the two peaks do not correlate with the respective boundaries of L1 and L2 showed in [19]. The largest peak is centered at 40 ka and comprises 16 samples labeled L1 and 9
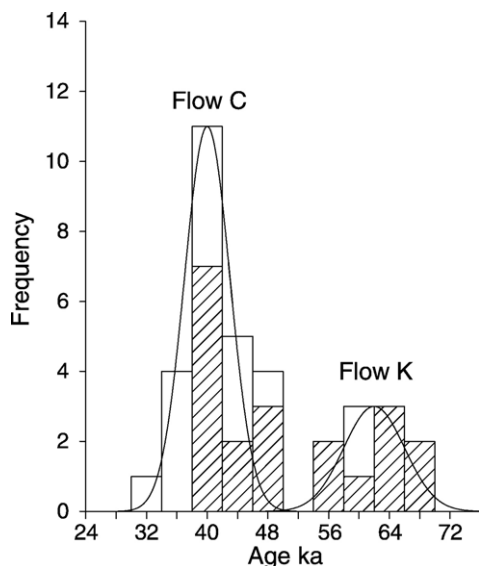
Fig. 4. Histogram of lava flow ages from Mauna Kea, HI showing two distinct peaks corresponding to flows *C* and *K*. Striped bars indicate samples labeled L2 and open bars show the total frequency for samples labeled L1 and L2. The solid lines give the Gaussian frequency distributions corresponding to mean ages of 40 and 62 ka, and respective standard deviations of 3 kyr and 4 kyr, normalized to the peak frequencies.

samples labeled L2. Our interpretation is that the L1 flow is more laterally extensive than is suggested by the geologic map, and that the samples constituting the L1 peak represent a single flow at 40 ka. Although the possibility that the L1 peak represents more than one flow cannot be eliminated based on chemical analyses or field appearances of samples due to similarities between Laupahoehoe flows of widely different ages, there are several other observations that we discuss below that support our interpretation. We refer to the laterally extensive flow erupted at 40 ka and consisting of samples labeled both L1 and L2 as flow *C*.

Another grouping of ages centered at 62 ka and consisting of 10 samples represents an older flow erupted mostly to the east of flow *C*. The flow appears occasionally as unmapped kipukas (older outcrops surrounded by younger lava) that are surrounded by flow *C*. Because this histogram peak is clearly distinct from the 40 ka peak, this second flow can be easily distinguished from flow *C* on the basis of ^{36}Cl ages alone. We refer to the older flow as flow *K*.

Samples that plotted midway between the peaks were removed from the data set on the basis that they could not be clearly assigned to either flow. This meant removing three samples (HAW00-19, HAW00-22 and HAW03-57) that yielded ages outside of three sample

standard deviations from the mean age of either flow. These outliers could be explained as eroded/exhumed samples from flow *C*, which, because of the double exponential depth-dependence for neutron activation reactions [28], could make these samples appear too old. Sample HAW00-16 is also anomalous, giving an age of 19.6 ± 1.7 ka for the 40 ka flow. This sample was taken from an ejecta block at the rim of a cinder cone composed of loose, easily erodible material. The young age for this sample may be a result of erosion of the cone. With these four outliers discarded, the spread of the *C* and *K* age distributions can mostly be explained by the analytical uncertainty in the AMS measurements. With the trimmed data set, the standard deviations of the sample age distributions from flows *C* and *K* are 4.1 and 4.3 kyr, which are slightly larger than the average analytical uncertainties for measurements on samples from the two flows ($\bar{\sigma}_C = 3.0$ kyr, $\bar{\sigma}_K = 3.7$ kyr). This suggests that geological processes such as erosion or burial that would add to the statistical spread of ages play a minor role, and supports our interpretation that only two lava flows are represented in this data set. If additional, inadvertently sampled flows are present in the trimmed data set then these flows are indistinguishable within the analytical precision of our measurements from flows *C* and *K*, and therefore should not affect the calculated atmospheric attenuation length.

Our interpretation of the histogram is consistent with observations on the spatial and temporal distribution of Laupahoehoe eruptions. The Laupahoehoe volcanic substage is characterized by relatively infrequent eruptions from point-source vents distributed over the upper flanks of Mauna Kea and marked by thick (commonly 5–10 m), laterally extensive aa flows [17]. The spatial and temporal separation of the flows makes it unlikely that two flows of similar age would occur in the same area. There are only three additional Laupahoehoe vents (indicated in Fig. 1 by vents with arrows showing flow direction) that could have produced flows capable of reaching any of our sample locations. The lowermost of these vents produced ash that partially covers flows *C* and *K* and therefore a flow from this vent would yield younger ages if mistakenly sampled. The anomalous ages are mostly older than flow *C*, however, and therefore cannot be related to this vent. The two other vents are at higher elevations and could have affected a broader area. Because the Laupahoehoe substage lasted at least 60 kyr and produced only three additional flows that could have contributed to our data set, we would expect that samples from these flows would be easily identified as outliers unless eruptions were contemporary.

Another line of evidence that supports our interpretation is the lack of correlation between sample age and location. The correlation between the spatial separation (lag distance) of pairs of samples and the difference in age between those samples is negligible, with $R < 0.01$. If we had erroneously sampled flow surfaces with ages different from C and K, then we would expect that samples taken close together should tend to give ages in better agreement with each other than with samples from farther away since samples from the same small area would more likely represent the same flow. The low correlation coefficient indicates that there is no significant spatial clustering of ages. That some samples can be in poor agreement with nearby samples despite unequivocal field evidence that all samples are from the same flow is demonstrated by samples HAW03-56, 57 and 58 which yield ages of 45.5 ± 3.0, 47.9 ± 1.9, and 39.6 ± 1.8 ka. In this case sample HAW03-57 is a clear outlier (at 4σ) from the flow C distribution, whereas samples HAW03-56 and HAW03-58 agree to within 1.7σ and $< 1\sigma$ with the mean age for flow C. The flow surface is visually continuous between the three samples and the anomalous age cannot be explained as a kipuka from an earlier eruption. This sample was one of four outliers removed from the data set based on statistical considerations.

4.2. Atmospheric attenuation length for ^{36}Cl production

The attenuation length for ^{36}Cl production was determined by choosing Λ (the only free parameter) such that the sum of the weighted least-square (χ^2) deviations [29] between sample ages for distributions C and K was minimized. This yields the value of Λ that most effectively reduces the spread of lava flow ages for samples from both lava flows (Fig. 5). The value of $\Lambda = 138 \pm 5$ g cm^{-2} gives the best fit to the entire data set, and independent fits to flows K and C yield $\Lambda_C = 137 \pm 6$ g cm^{-2} and $\Lambda_K = 139 \pm 8$ g cm^{-2}. Uncertainties are 1σ (68.3%), which, for one degree of freedom corresponds to $\Delta\chi^2 = 1$ [29]. Apparent ages (Table 1) and the best fit attenuation length from the procedure above are shown in Fig. 6.

The attenuation length from Mauna Kea lava flows is only slightly sensitive to the choice of production rates. This small sensitivity is related to the variability in Cl content between samples, which makes the scatter of apparent ages dependent on the choice of production rates. Using production rates from [30] for potassium and calcium and the $P_f(0)$ value from [21] yields an attenuation length that is only 1% lower, while using only production rates from [21] yields a
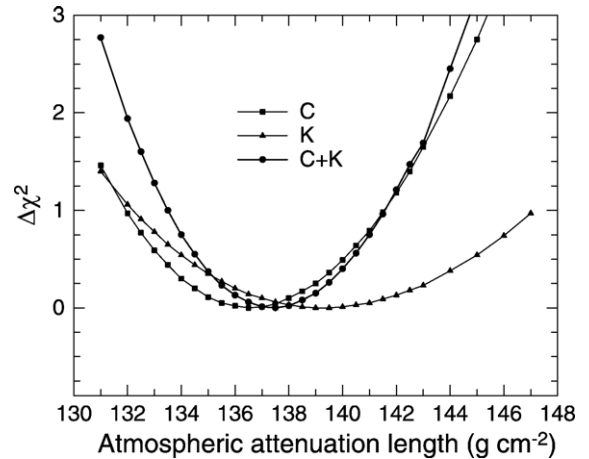

Fig. 5. Best fit Λ determined by minimizing the χ^2 deviation of lava flow ages.

value that is 1% higher. Only the anomalous production rates from [31] affect Λ significantly, giving a value that is 4% lower. The value of Λ that we report is based on [21]'s calibration data, rescaled to sea level and high latitude using the most updated scaling formulation [16]. This choice of calibrated production rates is justified by the fact that [21] has the largest number of calibration sites, and is supported by the observation that those values give the smallest spread in the sample age distributions.

How robust is our determination of Λ? Removing any single sample does not change the value of the attenuation length by more than 2%. Including any one of the three samples that were excluded from flow C because they plot between the histogram peaks (HAW00-19, HAW00-22 and HAW03-57) also does not change the attenuation length by more than 2%, and including these three samples in flow C gives the same value as excluding them. Including samples HAW00-19 and HAW00-22 in flow K also does not change Λ, although if sample HAW03-57 is also included in K lambda becomes 7% higher. However, it is clear based on our field observations (which indicate that flow surface where sample HAW03-57 was collected is continuous with samples HAW03-56 and HAW03-58, both of which plot clearly in C) and from statistical arguments (age of HAW03-57 is > 4 s from the mean age of K) that this sample should not be included with K.

4.3. Final corrected lava flow ages

Corrections for changes in geomagnetic dipole intensity and sea level over the exposure period have a large

Table 1
36Cl ages of Mauna Kea lava flow samples

	Average paleo elevation (m)	Uncorrected age (kyr)	Corrected age (kyr)	Apparent age (kyr)
HAW00-1-L1	3617	42.5 ± 5.0	33.8 ± 4.0	61.9 ± 7.1
HAW00-2-L1	3485	51.6 ± 2.4	41.0 ± 1.9	68.8 ± 3.0
HAW00-3-L1	3415	53.9 ± 1.7	42.7 ± 1.3	68.5 ± 2.1
HAW00-4-L1	3278	49.1 ± 3.7	38.4 ± 2.8	57.0 ± 4.0
HAW00-6-L1	3001	61.9 ± 6.0	48.4 ± 4.6	59.8 ± 5.4
HAW00-8-L1	2303	45.8 ± 4.0	35.7 ± 3.1	28.1 ± 2.3
HAW00-9-L1	2322	46.9 ± 3.8	36.5 ± 2.9	29.1 ± 2.2
HAW00-10-L1	2137	71.8 ± 25.0	53.1 ± 18.0	36.3 ± 11.6
HAW00-13-L1	2861	55.8 ± 5.8	43.9 ± 4.6	49.7 ± 4.9
HAW00-14-L1	2772	50.8 ± 5.4	40.0 ± 4.3	42.9 ± 4.4
HAW00-15-L1	2639	61.4 ± 4.4	47.5 ± 3.3	46.3 ± 3.1
HAW00-16-L2	3256	25.7 ± 2.2	20.6 ± 1.8	30.8 ± 2.6
HAW00-17-L2	3198	93.9 ± 5.5	70.9 ± 4.0	96.0 ± 5.2
HAW00-18-L2	3041	61.7 ± 5.2	48.5 ± 4.0	61.4 ± 4.9
HAW00-19-L2	2802	69.5 ± 5.2	54.2 ± 4.0	58.4 ± 4.1
HAW00-20-L2	2660	78.7 ± 5.5	58.9 ± 4.0	56.9 ± 3.6
HAW00-21-L2	2098	93.4 ± 5.6	69.1 ± 4.0	45.1 ± 2.4
HAW00-22-L2	2205	67.5 ± 3.6	52.4 ± 2.8	37.8 ± 1.9
HAW00-23-L2	2241	91.6 ± 5.5	68.3 ± 4.0	49.3 ± 2.7
HAW00-24-L2	2381	91.6 ± 7.9	67.7 ± 5.6	53.9 ± 4.1
HAW00-25-L2	2513	86.8 ± 5.0	65.0 ± 3.7	56.8 ± 3.1
HAW00-27-L2	1994	80.0 ± 5.9	59.8 ± 4.4	36.6 ± 2.6
HAW03-55-L1	3215	59.2 ± 3.2	46.5 ± 2.5	65.8 ± 3.4
HAW03-56-L2	3089	60.9 ± 4.1	48.0 ± 3.2	62.6 ± 4.2
HAW03-57-L2	3044	64.6 ± 2.6	50.5 ± 2.0	63.9 ± 2.4
HAW03-58-L2	3020	53.1 ± 2.5	41.7 ± 1.9	52.5 ± 2.4
HAW03-59-L1	3188	82.5 ± 3.3	62.5 ± 2.4	84.9 ± 3.2
HAW03-60-L2	2368	53.0 ± 3.3	40.8 ± 2.4	33.4 ± 1.8
HAW03-61-L2	2367	54.3 ± 9.4	42.4 ± 7.2	34.6 ± 5.6
HAW03-62-L2	2309	96.9 ± 5.3	72.2 ± 3.9	54.4 ± 2.8
HAW03-63-L2	2508	56.1 ± 3.2	43.4 ± 2.4	37.6 ± 2.0
HAW03-64-L2	2516	52.9 ± 2.9	41.0 ± 2.2	37.1 ± 1.9
HAW03-65-L2	2101	55.4 ± 3.2	43.4 ± 2.5	29.4 ± 1.7
HAW03-66-L2	2132	56.3 ± 3.6	43.7 ± 2.8	30.3 ± 1.9
HAW03-67-L1	2082	48.5 ± 2.7	37.4 ± 2.0	25.2 ± 1.3
HAW03-68-L1	2063	64.4 ± 3.1	49.3 ± 2.3	32.3 ± 1.4
HAW03-69-L1	2128	83.8 ± 3.8	62.6 ± 2.7	42.1 ± 1.7

Corrected ages have been corrected for paleomagnetic dipole strength variations, isostatic sinking sea level changes and are based on production rates that have also been corrected for the same effects. Uncorrected ages neglect the corrections above and are based on uncorrected production rates. Apparent ages are calculated by assuming that all samples have the same elevation and by neglecting radioactive decay. The apparent age is directly proportional to the 36Cl production rate in the sample.

impact on sample ages. Final corrected lava flow ages were calculated using the best fit attenuation length of 138 g cm^{-2} and the latitude scaling in [6]. Exposure ages on individual samples are given in Table 1. The mean exposure ages for flows C and K are 40.1 ± 0.6 and 62.2 ± 1.0 ka (uncertainties are standard error of the mean). These ages are 9.5 and 17.8 kyr lower than the uncorrected ages, with 60–70% of the difference between

corrected and uncorrected ages being explained by the geomagnetic correction and the remainder being explained by isostatic sea-level corrections. The geomagnetic correction is nearly the same for both lava flows because the integrated field intensity is nearly the same in the range 40–60 ka, whereas the elevation correction is greater for flow K because subsidence is assumed to be a linear function of time. Our calculations demonstrate that corrections for paleomagnetic and paleo-elevation changes should not be neglected at Hawaii.

4.4. Comparison of lava flow data with neutron flux scaling model

Elevation profiles in naturally irradiated materials provide an opportunity to validate production rate scaling models derived from measurements of cosmic-ray nucleon fluxes. The attenuation length determined from Hawaiian lava flows ($\Lambda = 138 \pm 5$ g cm^{-2}) corresponds to the paleo-elevation range 3.7–2.1 km and to an average paleo $R_C = 11$ GV. According to [6,16], Λ for the energetic nucleon component is 140 g cm^{-2}, and Λ for the low energy component is 149 g cm^{-2} for 3.7–2.1 km and $R_C = 11$ GV. The lava flow samples reported in this work incorporate both high- and low-energy production of 36Cl, with a variable, but on average nearly equal contribution from the three major reactions: spallation of calcium, spallation of potassium and thermal neutron activation of 35Cl. The effective attenuation length for
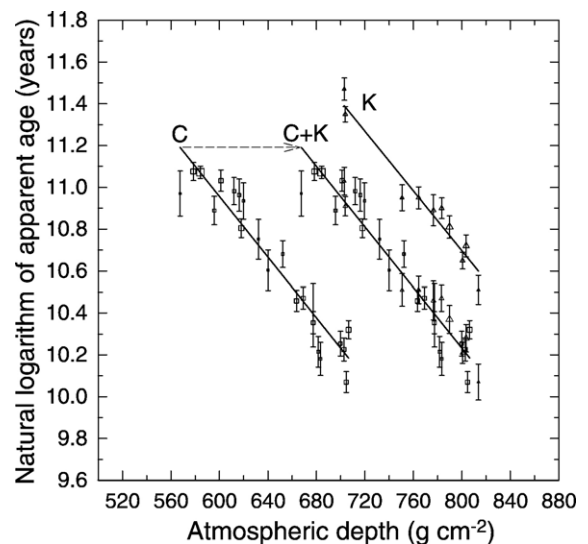

Fig. 6. Natural logarithm of apparent lava flow age versus atmospheric depth (symbols) and best fit attenuation lengths (lines). Flows C and K are plotted together ($C+K$) by normalizing the age of flow K to flow C. Data for flow C are displaced to the left by 100 g cm^{-2} for clarity. Error bars are 1σ and symbol sizes are inversely proportional to the error bars.

[36]Cl production corresponding to the average spallation/neutron activation ratio of our samples and to the average paleo rigidities and paleo elevations of the lava flows is $\Lambda = 144$ g cm^{-2}, which is consistent to within 2σ error limits with the value we measured in Mauna Kea lava flows. Although our results support the use of neutron flux measurements to scale production rates, the lava flow data presented here are not precise enough to answer the fundamental question of whether scaling functions depend on energy [6,16].

The agreement between our geologically derived Λ and neutron flux measurements confirms that spallation by nucleons and thermal neutron activation are the dominant [36]Cl production mechanisms over the altitude range of these lava flows. An important mechanism near sea level is slow negative muon capture by calcium [32]. Because slow muons are more highly penetrating (Λ_μ of ~ 240 g cm^{-2} [34]) than nucleon fluxes, the effective Λ for nuclide production would be significantly greater if muon interactions were an important pathway in these samples for [36]Cl production. The production rate in calcium by slow-muons has been determined to be 10% of the sea-level high-latitude production rate, but is not known for potassium [32]. Assuming that calcium is the only target for muon capture, only 2% of the [36]Cl production in the lowest elevation samples should be from slow muon reactions, which would not appreciably affect the atmospheric attenuation length we measured in Hawaii. Our data are consistent with [32]'s work in that we found no evidence for a greater muon contribution.

5. Conclusions

We determined the low-latitude elevation dependence of production rates by measuring cosmogenic [36]Cl in two Hawaiian lava flows. The elevation profile is best represented by an atmospheric attenuation length of 138 ± 5 g cm^{-2} which corresponds to an average paleo R_C of 11 GV and paleo-elevation range of 2100–3700 m over the exposure period. The effective attenuation lengths determined from cosmic-ray surveys ($R_C = 11$ GV, 2100–3700 m) are 140 g cm^{-2} for high-energy nucleons and 149 g cm^{-2} for low-energy neutrons. The overall value for the Hawaiian lava flows, which have a contribution from both high- and low-energy reactions, is 144 g cm^{-2}, which is within the 2σ error limits of the value we measured in Mauna Kea lava flows.

Determining scaling factors directly from cosmogenic nuclide buildup in natural landforms is a challenging task. Except for relatively short-lived nuclides, where in slowly eroding landforms decay outpaces erosion [33], this type of work requires either an extensive, well-delineated, monogenetic landform or several independently calibrated landforms spanning a large elevation range. There are few locations where these restrictive conditions are met. Furthermore, because steep climate gradients are usually associated with steep topographic gradients, surface preservation along a profile can be highly variable.

A fundamental shortcoming of the geological approach is that scaling functions are not necessarily transferable between nuclides. The main problem is that excitation functions and muogenic and radiogenic contributions are different for different nuclides. Considering the effort required in obtaining a reliable elevation profile for a single nuclide at just one location, it is clear that geological profiles such as the one described here cannot replace the high-precision and global coverage of neutron flux surveys. Instead, geological profiles should be used to check the validity of using neutron flux measurements to scale production rates for a given nuclide. However, naturally irradiated artificial targets, when feasible, may provide a better opportunity to address fundamental questions related to scaling factors because geological uncertainties can be eliminated. Understanding the relation between neutron measurements and cosmogenic nuclide production requires a combination of target experiments, natural calibration work, neutron flux measurements and nucleonic cascade modeling. Improving the accuracy of scaling functions through work these areas remains a goal of the new CRONUS-Earth initiative (USA) and its European counterpart, CRONUS-Europe.

Appendix A. Supplementary Material

Supplementary data associated with this article can be found, in the online version, at doi:10.1016/j.epsl.2006.03.050.

References

[1] J.C. Gosse, F.M. Phillips, Terrestrial cosmogenic nuclides: theory and application, Quaternary Science Reviews 20 (2001) 1475–1560.

[2] D. Lal, Cosmic ray labeling of erosion surfaces: in situ nuclide production rates and erosion models, Earth and Planetary Science Letters 104 (1991) 424–439.

[3] D. Lal, B. Peters, Cosmic ray produced radioactivity on earth, in: K. Sitte (Ed.), Encyclopedia of Physics: Cosmic Rays II, Encyclopedia of Physics, vol. 46/2Springer-Verlag, Berlin, 1967, pp. 551–612.

[4] T.J. Dunai, Scaling factors for production rates of in situ produced cosmogenic nuclides: a critical reevaluation, Earth and Planetary Science Letters 176 (2000) 157–169.

[5] N. Lifton, A robust scaling model for in situ cosmogenic nuclide production rates, Geological Society of America, Annual Meeting, Abstracts with Programs, Reno, Nevada, 2000, p. A400.

[6] D. Desilets, M. Zreda, Spatial and temporal distribution of secondary cosmic-ray nucleon intensity and applications to in situ cosmogenic dating, Earth and Planetary Science Letters 206 (2003) 21–42.

[7] D. Desilets, M. Zreda, On scaling cosmogenic nuclide production rates for altitude and latitude using cosmic-ray measurements, Earth and Planetary Science Letters 193 (2001) 213–225.

[8] D. Lal, J.R. Arnold, H. Masatake, Cosmic-ray production of ^{7}Be in oxygen and ^{32}P, ^{33}P, ^{35}S in Argon at mountain altitudes, Physical Review 118 (1964) 1626.

[9] H. Mabuchi, G. Reisuke, W. Yukio, H. Hiroshi, Phosphorous-32 induced by atmospheric cosmic rays in laboratory chemicals, Geochemical Journal 4 (1971) 105–110.

[10] E.T. Brown, T.W. Trull, P. Jean-Baptiste, G. Raisbeck, D. Bourlès, F. Yiou, B. Marty, Determination of cosmogenic production rates of ^{10}Be, ^{3}He and ^{3}H in water, Nuclear Instruments and Methods in Physics Research B 172 (2000) 873–883.

[11] M. Kurz, Cosmogenic helium in a terrestrial igneous rock, Nature 320 (1986) 435–439.

[12] E.T. Brown, E.J. Brook, G.M. Raisbeck, F. Yiou, M.D. Kurz, Effective attenuation lengths of cosmic-rays producing ^{10}Be and ^{26}Al in quartz — implications for exposure age dating, Geophysical Research Letters 19 (4) (1992) 369–372.

[13] M.G. Zreda, F.M. Phillips, D. Elmore, P.W. Kubik, P. Sharma, R.I. Dorn, Cosmogenic chlorine-36 production rates in terrestrial rocks, Earth and Planetary Science Letters 105 (1991) 94–109.

[14] H. Carmichael, M.A. Shea, R.W. Peterson III, Cosmic-ray latitude survey in Western USA and Hawaii in summer, 1966, Canadian Journal of Physics 47 (1969) 2057–2065.

[15] H. Carmichael, R.W. Peterson, Dependence of the neutron monitor attenuation coefficient on atmospheric depth and on geomagnetic cutoff in 1966 and in 1970, Proceedings of the 12th International Cosmic Ray Conference, 1971, pp. 887–892.

[16] D. Desilets, M. Zreda, T. Prabu, Extended scaling factors for in-situ cosmogenic nuclides: new measurements at low latitude, Earth and Planetary Science Letters 246 (2006-this issue) 265–276, doi:10. 1016/j.epsl.2006.03.051.

[17] E.W. Wolfe, W.S. Wise, G.B. Dalrymple, The Geology and Petrology of Mauna Kea Volcano, Hawaii — A Study of Postshield Volcanism, United States Geological Survey, Washington, 1997, 129 pp.

[18] S.P. Juvik, J.O. Juvik, T.R. Paradise, Atlas of Hawaii, University of Hawaii Press, Honolulu, 1998.

[19] E.W. Wolfe, J. Morris, Geologic Map of the Island of Hawaii, USGS, 1996.

[20] D. Desilets, M. Zreda, P.F. Almasi, D. Elmore, Determination of cosmogenic ^{36}Cl in rocks by isotope dilution: innovations, validation and error propagation, Chemical Geology (in press).

[21] F.M. Phillips, W.D. Stone, J.T. Fabryka-Martin, An improved approach tocalculating low-energy cosmic-ray neutron fluzes near the land/atmosphere interface, Chemical Geology 175 (2001) 689–701.

[22] Y. Guyodo, J.P. Valet, Global changes in intensity of the Earth's magnetic field during the past 800 kyr, Nature 399 (1999) 249–252.

[23] S. Yang, H. Odah, J. Shaw, Variations in the geomagnetic dipole moment over the last 12 000 years, Geophysical Journal International 140 (2000) 158–162.

[24] K.R. Ludwig, B.J. Szabo, J.G. Moore, K.R. Simmons, Crustal subsidence rate off Hawaii determined from ^{234}U/^{238}U ages of drowned coral reefs, Geology 19 (1991) 171–174.

[25] NOAA, National Climatic Data Center radiosonde database available on-line [http://raob.fsl.noaa.gov/].

[26] J.O. Stone, Air pressure and cosmogenic isotope production, Journal of Geophysical Resarch 105 (B10) (2000) 23753–23759.

[27] Manual of the ICAO Standard Atmosphere extended to 80 kilometres (262 500 feet), International Civil Aviation Organi- sation, Doc. 7488, 1993.

[28] B. Liu, F.M. Phillips, J.T. Fabryka-Martin, M.M. Fowler, R.S. Biddle, Cosmogenic ^{36}Cl accumulation in unstable landforms, 1. Effects of the thermal neutron distribution, Water Resources Research 30 (11) (1994) 3115–3125.

[29] W.H. Press, B.P. Flannery, S.A. Teukolsky, W.T. Vetterling, Numerical Recipes, University of Cambridge, New York, 1980, 818 pp.

[30] J. Stone, J. Evans, K. Fifield, R. Cresswell, G. Allan, Cosmogenic chlorine-36 production rates from calcium and potassium, Radiocarbon 38 (1996) 170–171.

[31] T.W. Swanson, M.L. Caffee, Determination of ^{36}Cl production rates derived from the well-dated deglaciation surfaces of Whidbey and Fidalgo Islands, Washington, Quaternary Research 56 (2001) 366–382.

[32] J.O.H. Stone, J.M. Evans, L.K. Fifield, G.L. Allan, R.G. Cresswell, Cosmogenic chlorine-36 production in calcite by muons, Geochi- mica et Cosmochimica Acta 62 (3) (1998) 433–454.

[33] N. Lifton, J.S. Pigati, A.J.T. Jull, J. Quade, Testing cosmogenic nuclide production rate scaling models using in situ cosmogenic ^{14}C from surfaces at secular equilibrium: preliminary results, Eos Transactions, AGU Fall Meeting Supplement, 2002.

[34] B. Rossi, M. Sands, R.F. Sard, Measurements of slow meson intensity at several altitudes, Physical Review 72 (1947) 120–125.